The mechanism of hydrosilylation (Fig. 2) can be tentatively visualized as a modified ionic hydrogenation mechanism, which has been previously formulated for similar catalysts[27,28]. Trialkylsilyl cation (silylium ion) is transferred from the metal to the ketone, yielding a carbocation intermediate. The carbocation abstracts a hydride (H^-) from $HSiEt_3$ or from the metal, furnishing alkoxysilane and closing the catalytic cycle. The transfer of silylium and hydride ions could be concerted to some degree, but the observed cationic rearrangement in the reaction of cyclopropyl methyl ketone indicates an appreciable contribution of a cationic intermediate. A more detailed mechanistic investigation is needed to expand upon these preliminary findings.

The method for catalyst recycling and recovery presented here offers significant advantages, since it is solvent-free and requires no temperature changes, but this strategy is also prone to limitations. Examples of catalyst self-separation demonstrated thus far are restricted to aliphatic substrates, and the solvent-free approach is limited to both substrates being liquids. A challenge for future development is to tailor catalysts and hydrosilanes with the aim of engaging a broader scope of substrates into such solvent-free reactions with catalyst self-separation. A more general goal is to understand the fundamental aspects of liquid clathrate formation and to convert other catalysts into 'clathrate-enabled' catalysts, broadening the potential applicability of this recovery method to other classes of substrates and reactions. □

Received 11 April; accepted 23 June 2003; doi:10.1038/nature01856.

1. Gladysz, J. A. Introduction: Recoverable catalysts and reagents–perspective and prospective. *Chem. Rev.* **102**, 3215–3216 (2002).
2. Gladysz, J. A. Recoverable catalysts. Ultimate goals, criteria of evaluation, and the green chemistry interface. *Pure Appl. Chem.* **73**, 1319–1324 (2001).
3. Cole-Hamilton, D. J. Homogeneous catalysis — new approaches to catalyst separation, recovery, and recycling. *Science* **299**, 1702–1706 (2003).
4. Kragl, U. & Dwars, T. The development of new methods for the recycling of chiral catalysts. *Trends Biotechnol.* **19**, 442–449 (2001).
5. Horváth, I. T. Fluorous biphase chemistry. *Acc. Chem. Res.* **31**, 641–650 (1998).
6. Gladysz, J. A. & Curran, D. P. Fluorous chemistry: From biphasic catalysis to a parallel chemical universe and beyond. *Tetrahedron* **58**, 3823–3825 (2002).
7. Zuwei, X., Ning, Z., Yu, S. & Li, K. Reaction-controlled phase-transfer catalysis for propylene epoxidation to propylene oxide. *Science* **292**, 1139–1141 (2001).
8. Hourdin, G., Germain, A., Moreau, C. & Fajula, F. The catalysis of the Ruff oxidative degradation of aldonic acids by copper(II)-containing solids. *J. Catal.* **209**, 217–224 (2002).
9. Wang, Y., Jiang, J., Zhang, R., Liu, X. & Jin, Z. Thermoregulated phase transfer ligands and catalysis IX. Hydroformylation of higher olefins in organic monophase catalytic system based on the concept of critical solution temperature of the nonionic tensioactive phosphine ligand. *J. Mol. Catal. A* **157**, 111–115 (2000).
10. Wende, M., Meier, R. & Gladysz, J. A. Fluorous catalysis without fluorous solvents. *J. Am. Chem. Soc.* **123**, 11490–11491 (2001).
11. Wende, M. & Gladysz, J. A. Fluorous catalysis under homogeneous conditions without fluorous solvents: A "greener" catalyst recycling protocol based upon temperature-dependent solubilities and liquid/solid phase separation. *J. Am. Chem. Soc.* **125**, 5861–5872 (2003).
12. Ishihara, K., Kondo, S. & Yamamoto, H. 3,5-Bis(perfluorodecyl)phenylboronic acid as an easily recyclable direct amide condensation catalyst. *Synlett* 1371–1374 (2001).
13. Ishihara, K., Hasegawa, A. & Yamamoto, H. A fluorous super Bronsted acid catalyst: Application to fluorous catalysis without fluorous solvents. *Synlett* 1299–1301 (2002).
14. Xiang, J. N., Orita, A. & Otera, J. Fluoroalkyldistannoxane catalysts for transesterification in fluorous biphase technology. *Adv. Synth. Catal.* **344**, 84–90 (2002).
15. Atwood, J. L. in *Coordination Chemistry of Aluminum* (ed. Robinson, G. H.) 197–232 (VCH, New York, 1993).
16. Steed, J. W. & Atwood, J. L. *Supramolecular Chemistry* 707 (Wiley, Chichester, 2002).
17. Anastas, P. T. & Kirchhoff, M. M. Origins, current status, and future challenges of green chemistry. *Acc. Chem. Res.* **35**, 686–694 (2002).
18. Anastas, P. T. & Zimmerman, J. B. Design through the 12 principles of green engineering. *Environ. Sci. Technol.* **37**, 94A–101A (2003).
19. DeSimone, J. M. Practical approaches to green solvents. *Science* **297**, 799–803 (2002).
20. Holbrey, J. D. *et al.* Liquid clathrate formation in ionic liquid–aromatic mixtures. *Chem. Commun.* 476–477 (2003).
21. Lambert, J. B., Zhao, Y., Wu, H., Tse, W. C. & Kuhlmann, B. The allyl leaving group approach to tricoordinate silyl, germyl, and stannyl cations. *J. Am. Chem. Soc.* **121**, 5001–5008 (1999).
22. Korolev, A. V., Ihara, E., Young, V. G. Jr & Jordan, R. F. Cationic aluminum alkyl complexes incorporating aminotroponiminate ligands. *J. Am. Chem. Soc.* **123**, 8291–8309 (2001).
23. Borovik, A. S. & Barron, A. R. Arene-mercury complexes stabilized by aluminum and gallium chloride: Catalysts for H/D exchange of aromatic compounds. *J. Am. Chem. Soc.* **124**, 3743–3748 (2002).
24. Ojima, I. in *The Chemistry of Organic Silicon Compounds* (eds Patai, S. & Rappoport, Z.) 1479–1526 (Wiley, New York, 1989).
25. Ojima, I., Li, Z. & Zhu, J. in *The Chemistry of Organic Silicon Compounds, Vol. 2* (eds Rappoport, Z. & Apeloig, Y.) 1687–1792 (Wiley, New York, 1998).
26. Dioumaev, V. K., Szalda, D. J., Hanson, J., Franz, J. A. & Bullock, R. M. An N-heterocyclic carbene as a bidentate hemilabile ligand: A synchrotron X-ray diffraction and density functional theory study. *Chem. Commun.* 1670–1671 (2003).
27. Bullock, R. M. & Voges, M. H. Homogeneous catalysis with inexpensive metals: Ionic hydrogenation of ketones with molybdenum and tungsten catalysts. *J. Am. Chem. Soc.* **122**, 12594–12595 (2000).
28. Voges, M. H. & Bullock, R. M. Catalytic ionic hydrogenations of ketones using molybdenum and tungsten complexes. *J. Chem. Soc. Dalton Trans.* 759–770 (2002).

Supplementary Information accompanies the paper on **www.nature.com/nature**.

Acknowledgements This research was supported by the Division of Chemical Sciences, Office of Basic Energy Sciences, of the US Department of Energy.

Competing interests statement The authors declare that they have no competing financial interests.

Correspondence and requests for materials should be addressed to M.B. (bullock@bnl.gov).

Southern Ocean origin for the resumption of Atlantic thermohaline circulation during deglaciation

Gregor Knorr[1,2] **& Gerrit Lohmann**[1,2]

[1]*Institut für Meteorologie, Universität Hamburg, Bundesstrasse 55, 20146 Hamburg, Germany*
[2]*Fachbereich für Geowissenschaften und Forschungszentrum Ozeanränder, Universität Bremen, PO 330 440, 28334 Bremen, Germany*

During the two most recent deglaciations, the Southern Hemisphere warmed before Greenland[1,2]. At the same time, the northern Atlantic Ocean was exposed to meltwater discharge[3], which is generally assumed to reduce the formation of North Atlantic Deep Water[4,5]. Yet during deglaciation, the Atlantic thermohaline circulation became more vigorous, in the transition from a weak glacial to a strong interglacial mode[6]. Here we use a three-dimensional ocean circulation model[7] to investigate the impact of Southern Ocean warming and the associated sea-ice retreat[8] on the Atlantic thermohaline circulation. We find that a gradual warming in the Southern Ocean during deglaciation induces an abrupt resumption of the interglacial mode of the thermohaline circulation, triggered by increased mass transport into the Atlantic Ocean via the warm (Indian Ocean) and cold (Pacific Ocean) water route[9,10]. This effect prevails over the influence of meltwater discharge, which would oppose a strengthening of the thermohaline circulation. A Southern Ocean trigger for the transition into an interglacial mode of circulation provides a consistent picture of Southern and Northern hemispheric climate change at times of deglaciation, in agreement with the available proxy records.

Ice-core and ocean-sediment records reveal that during the last deglaciation, warming in the Southern Hemisphere preceded Greenland warming by more than 1,000 years (ref. 1), a time lag that was even longer for the penultimate deglaciation[2]. One candidate for an interhemispheric teleconnection is provided by the oceanic thermohaline circulation (THC). Proxy data[6] and modelling studies[7,11,12] indicate that the last deglaciation was characterized by a transition from a weak glacial to a strong interglacial Atlantic THC. During the Bølling–Allerød (B/A) warm period, the sea surface temperatures (SSTs) in the North Atlantic almost reached interglacial values, consistent with active deep water formation, corroborated by benthic $\delta^{13}C$ data[6]. While most studies investigate processes responsible for a shut-down of the THC, we consider the question of how the conveyor gets restarted after a glacial mode with

weak overturning, using a numerical model for interglacial and glacial background conditions (see Methods section).

For the present-day state, we obtain an Atlantic Ocean circulation with export of 14 Sv (1 Sv = 10^6 m^3 s^{-1}) at 30° S and maximum heat transport of 1.1 PW, which is in the range of observations[13]. For the Last Glacial Maximum (LGM), our modelled ocean circulation is characterized by a weaker circulation of about 8.5 Sv (Fig. 1a) and southward shifted convection sites (Fig. 1b), compared to present-day sites. North Atlantic Deep Water (NADW) is formed in the subpolar North Atlantic, and the North Atlantic Current flows in a zonal direction along the horizontal density gradients, consistent with reconstructions[6].

To simulate the resumption of the Atlantic THC during deglaciation, we assume a linear transition from glacial to interglacial values in Southern Ocean temperature, sea ice and wind stress over 1,500 years, consistent with a deglacial sea-ice retreat within 1,000 years in the Southern Ocean south of the present-day polar front[8]. Caused by Southern Ocean warming and accompanying sea-ice retreat, a strong increase in overturning circulation is detected in experiment LGM_100 (Fig. 2). The warming generates a negative density anomaly in the Southern Ocean, inducing anomalous westward velocities between 30° S and 50° S, consistent with geostrophic balance (Fig. 3a). Off the Brazilian coast, the anomalous flow is along with pressure gradients to the north. Part of the relatively warm and salty water originating from the Indian Ocean is directly injected into the subtropical South Atlantic via the eastern boundary current off the Namibian coast (Fig. 3). The thermal anomaly is attenuated along the northward conveyor route, but the saline characteristics of the warm water route persist[14] (Fig. 2b). The salinity increase in the upper layer of the North Atlantic preconditions NADW formation in a fashion comparable to a mechanism[9] that gradually intensifies convection during the first 1,000 years (Fig. 2b). The mechanism involves a positive feedback of THC owing to salinity advection[15]. Furthermore, sea-ice retreat in the Southern Ocean increases volume transport through the Drake Passage (25 Sv to 54 Sv) and the Atlantic import at 30° S of relatively cold and fresh water between 10° W and 50° W (Fig. 3).

Along with increased Atlantic overturning, the meridional heat transport warms the surface water of the North Atlantic, triggering an abrupt sea-ice retreat after 1,000 years. Besides the advective feedback, a convective feedback contributes to the resumption of the THC. Once convection is initiated in parts of the formerly ice-covered North Atlantic, the relatively warm and saline water masses from deeper layers coming up to the surface lose their heat readily, but keep their salt, and thus reinforce the starting process of convection (Fig. 2b). As a result, the mean convection depth in the Atlantic between 50° N and 60° N increases abruptly from 0 to

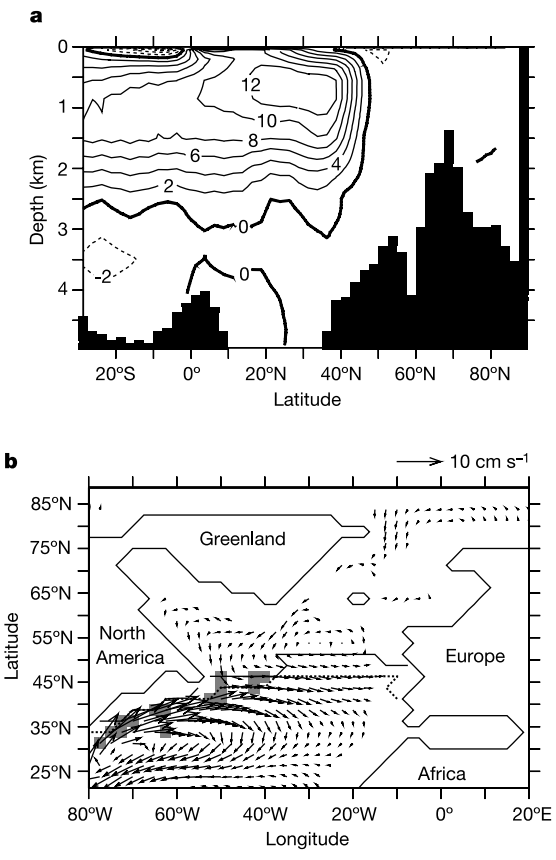

Figure 1 Modelled overturning streamfunction, as well as NADW convection sites and horizontal surface velocities in the Atlantic for the glacial control climate (LGM_CTRL). **a**, Meridional streamfunction (Sv); warm surface water flows northward to the subpolar regions, sinks, and flows southward as NADW, represented by the solid lines. **b**, Horizontal velocity (cm s^{-1}) in the upper 50 m of the North Atlantic. Major NADW convection sites are represented by the shaded area; summer and winter sea-ice margins are indicated by the solid and the dashed line, respectively.

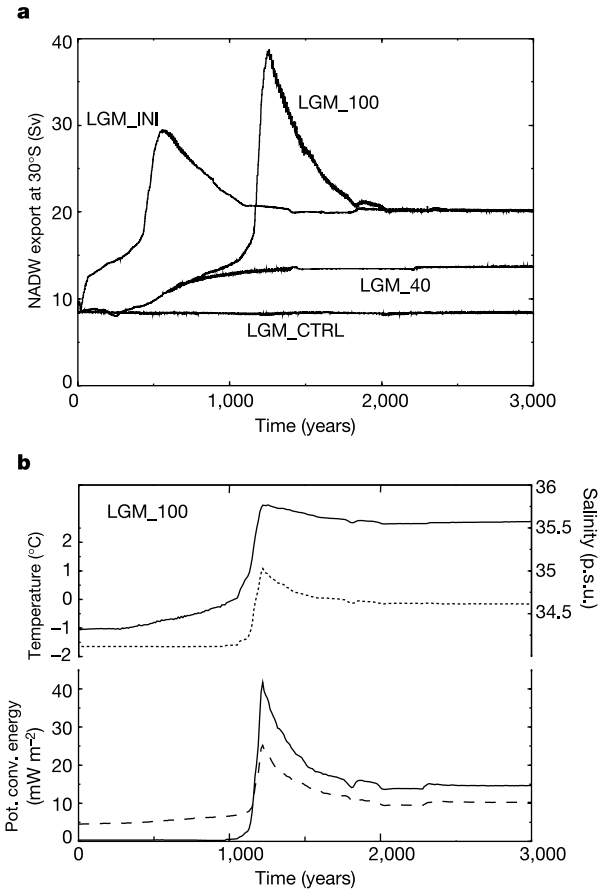

Figure 2 Temporal changes of NADW export at 30° S, and North Atlantic temperature, salinity and convection energy loss. **a**, In LGM_100, glacial conditions in the Southern Ocean (south of 30° S) are gradually replaced by interglacial conditions within 1,500 years. In LGM_40 gradual changes to interglacial conditions as in LGM_100 are assessed, but the transition terminates after 600 years, equivalent to a sea-ice retreat of 40%. Experiment LGM_INI represents instantaneously applied interglacial conditions of temperature, sea ice and wind stress. The curve LGM_CTRL shows the glacial control run. **b**, LGM_100 time series of SST (°C; dotted curve), salinity (p.s.u.; solid curve) and potential energy loss by convection (mW m^{-2}) in the North Atlantic averaged between 55° N and 65° N (solid curve) and between 40° N and 55° N (dashed curve).

140 m. The convection in large parts of the Labrador Sea is only temporarily active, whereas the convection sites south of Iceland remain in operation (see the animations in Supplementary Information). The maximum heat transport in the Atlantic Ocean increases from 0.8 PW to 1.6 PW after 3,000 model years, causing an SST rise of more than 6 K in the North Atlantic (Fig. 3b).

To investigate the abrupt warming in more detail, we have run experiment LGM_INI, where background conditions in the Southern Ocean are instantaneously switched from glacial to interglacial ones. The model response (Fig. 2a) is similar to LGM_100, indicating that the abrupt warming is independent on the timescale of sea-ice margin retreat in the Southern Ocean. In order to estimate the threshold for the nonlinear transition shown in Fig. 2a, a series of experiments with different sea-ice retreat scenarios in the Southern Ocean were performed, showing that ~50% sea-ice margin retreat from glacial to interglacial conditions is sufficient to cause the abrupt model response. Experiment LGM_40, with 40% sea-ice margin retreat, is representative of the experiments with a linear model response (Fig. 2a). Despite enhanced NADW formation in this experiment, the sea-ice margin in the North Atlantic is almost unaffected, and the feedback loop for the nonlinear resumption of the THC described above is not active, suggesting that the level of Southern Ocean warming governs the abrupt sea-ice retreat in the northern North Atlantic.

Furthermore, model simulations with alternated wind and temperature forcing reveal that imposed temperature and sea-ice changes in the Southern Hemisphere have a strong influence on THC strength compared to locally alternated wind fields. A further experiment showed that Northern Hemisphere warming has much less influence on NADW overturning strength than Southern Hemisphere warming (Supplementary Fig. 1).

In addition, we looked at the deglacial Heinrich sequence that is characterized by meltwater discharge to the North Atlantic[3], whose destabilizing impact on THC has been proposed to suppress warming in the north[16]. Our glacial reference state (LGM_CTRL) is monostable with respect to transient North Atlantic freshwater pulses[7,12], as revealed by experiment LGM_CTRL_H500 (Fig. 4). This explains the observed recovery of the reduced glacial THC after Heinrich events[6]. Different experiments with transient (LGM_SH_H500) and permanent (LGM_SH_Hperm) freshwater flow to the North Atlantic (Fig. 4a) show that the abrupt resumption of Atlantic THC via Southern Ocean warming prevails over the destabilizing impact of meltwater discharge during the Heinrich sequence. Compared to LGM_100, the overturning response in LGM_SH_H500 and LGM_SH_Hperm is damped in magnitude and delayed in time.

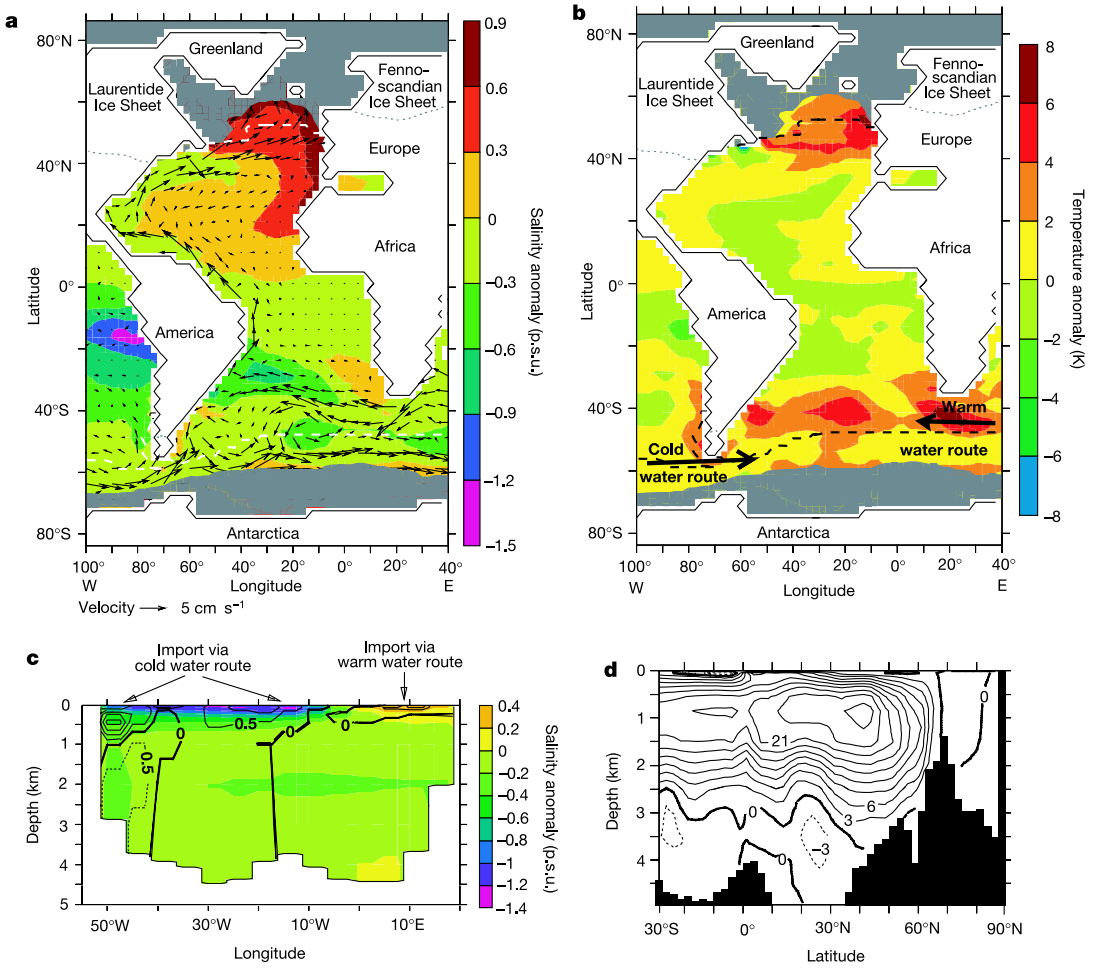

Figure 3 Differences between LGM_100 and LGM_CTRL, and meridional overturning streamfunction in LGM_100 after 3,000 model years. **a**, Annual mean salinity (p.s.u.) and horizontal velocity (cm s^{-1}) anomalies averaged over the upper 800 m. The grey shaded area and the dashed line show the annual mean 2 m height ice extent in experiment LGM_100 and LGM_CTRL, respectively. The maximum glacial continental ice margin is represented by the dotted lines. **b**, Annual mean temperature anomaly (K) averaged over the upper 50 m; schematically overlaid with the main pathways of water import to the Atlantic Ocean. Sea-ice margins and continental ice sheets as in **a**. **c**, Annual mean salinity anomaly (p.s.u.) and anomaly of the meridional velocity component (cm s^{-1}) at 30° S. Solid lines indicate northward flow, dashed lines represent southward flow. **d**, Meridional overturning streamfunction (Sv) in the Atlantic in LGM_100 after 3,000 model years.

So far, our investigations reveal that Southern Ocean warming and associated sea-ice retreat enhances the transport via warm and cold water routes, causing a THC flow regime that is stronger and bistable (Fig. 4b). The bistable flow regime is driven by heat loss, whereas freshwater tends to reduce overturning strength[15]. The restarted THC bears the potential to react to deglacial meltwater input to the North Atlantic with a substantial long-term THC weakening, in accordance with the Younger Dryas cold sequence[4,17] (Fig. 4b).

As a result of the restarted conveyor circulation (Fig. 3d), the maximum heat transport and the temperature in the North Atlantic increase dramatically (Fig. 3b), consistent with a temperature rise of more than 6 K for the B/A warm transition[18]. At the same time, temperatures in the tropical[17] and South Atlantic[19] decrease, in accordance with the oceanic interhemispheric teleconnection (increased THC cools the Southern Hemisphere[20]). In our model simulations, Southern Hemisphere cooling, as a response to a resumption of the THC in the North Atlantic, is inhibited by the experimental design. On the basis of the present investigation, the Antarctic Cold Reversal can be associated with an abrupt transition from a weak glacial to a strong interglacial ocean circulation mode that effectively transported heat to the North Atlantic. The corresponding B/A warm phase occurs only after a certain amount of heat has been transported to the North Atlantic, triggering a northern sea-ice retreat, which is then abruptly amplified by convective processes. We speculate that in conjunction with other effects[21,22], the increase in northward oceanic heat transport can contribute to the reduction of the great Northern Hemisphere ice sheets over North America and Scandinavia. The respective meltwater input weakens, but does not stop, NADW formation[23]. The involved mechanism is consistent with the phase offsets between Southern and Northern hemisphere climate change on Milankovitch timescales[1,2], and provides a possible explanation for the onset of the B/A. This mechanism represents an alternative explanation to the proposal that meltwater from Antarctica retracts Antarctic Bottom Water formation, leading to a switch-on of THC at a critical threshold[16], an effect that would amplify the mechanism proposed here.

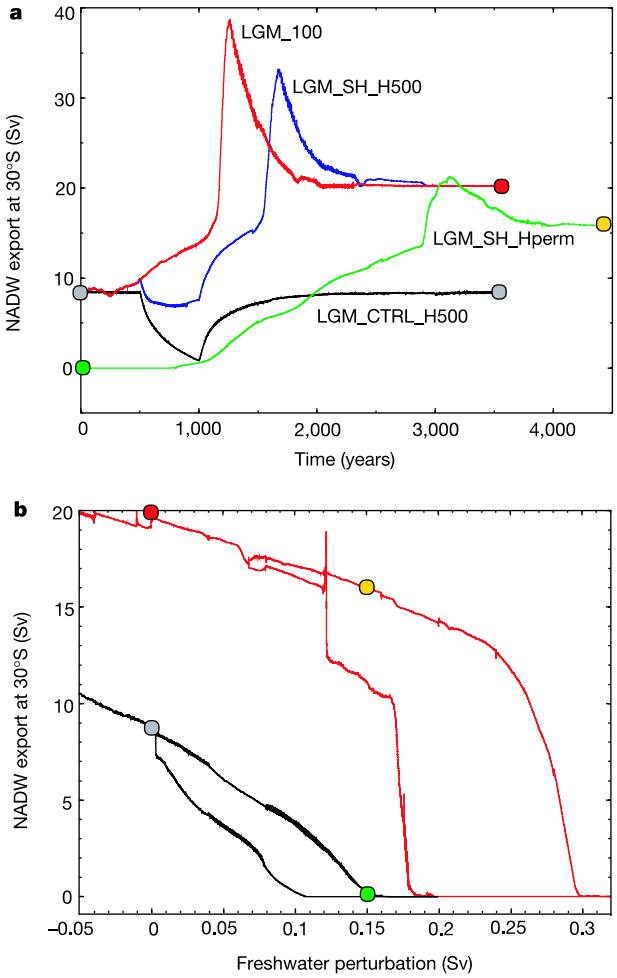

Figure 4 Atlantic NADW export at 30° S for the different freshwater pulse experiments and stability diagrams for the Atlantic THC. **a**, In LGM_CTRL_H500 and LGM_SH_H500, a transient freshwater pulse to the North Atlantic has been simulated between model year 500 and 1,000. In LGM_SH_perm, the freshwater input persists. Southern Ocean warming is applied in LGM_SH_H500 and LGM_SH_perm (also see Methods section). The coloured points indicate the different equilibrium climate states. **b**, The stability diagram (procedure explained in Methods section) of the glacial ocean circulation (black curve) differs substantially from that of LGM_100 (red curve). The restarted Atlantic THC exhibits a pronounced bistability for anomalous freshwater fluxes between +0.12 Sv and +0.3 Sv. The glacial THC shows a monostable behaviour at zero freshwater perturbation, and only weak bistability in the area of positive freshwater input. The location of climate states from **a** are displayed by the coloured points.

Our study suggests that the "Achilles Heel"[10] and the "Flywheel" of the Atlantic overturning circulation are located in the North Atlantic and the Southern Ocean, respectively. Interestingly, the tropical foraminifer *Globorotalia menardii* is re-seeded in the Atlantic Ocean at the last glacial–interglacial transition[24]. The only way to re-seed *G. menardii* in the Atlantic is around the Cape of Good Hope, leading to speculation[25] that the reopening of the Agulhas gap at the end of the last ice age may have played a role in restarting the Atlantic THC. Southern Ocean warming and associated sea-ice retreat might be the response to local Milankovitch forcing on the precessional period[26] or the result of tropical SST anomalies that transmitted from the tropical Pacific to the Antarctic region[27]. Since the South Atlantic is characterized by a number of unique dynamical features, such as the large Agulhas Rings that form a key link in the THC[9,28], it is of interest to investigate the mechanism proposed here, using high-resolution models of the South Atlantic region to obtain a more detailed view in this region. More well-dated high-resolution records from terrestrial and marine sites in the Southern Hemisphere will be needed to decipher these additional pathways. They seem to be necessary for the prediction of future climate scenarios with respect to rising atmospheric CO_2 concentration and its impact on the Atlantic overturning circulation. □

Methods

Model description

The ocean model is based on the three-dimensional large-scale geostrophic model LSG[5]. It includes a simple thermodynamic sea-ice model, a new advection scheme for temperature and salinity, and parameterization of overflow[29]. The horizontal resolution is 3.5° on a semi-staggered grid (type 'E') with 11 levels in the vertical. For glacial conditions the storage of water in inland ice sheets is taken into account by setting all ocean points with present-day water depth less than 120 m to land. This causes the Bering Strait to be closed, and several shallow areas like the Arctic shelves to become land. To drive the ocean, monthly fields of wind stress, surface air temperature and freshwater flux are taken from a present-day and LGM simulation of the atmospheric general circulation model ECHAM3/T42[30]. We use a hybrid coupled modelling approach, which allows an adjustment of surface temperatures and salinity to changes in the ocean circulation, based on an atmospheric energy balance model[29]. The applied heat flux parameterization has been shown to be a suitable choice, allowing the simulation of observed SSTs and the maintenance of large-scale temperature anomalies in perturbation experiments[29]. No flux correction is applied for both present-day and LGM boundary conditions.

Experimental design

In order to simulate the resumption of the Atlantic conveyor belt circulation after glacial times, we perform several experiments where interglacial values south of 30° S are applied as a surrogate for Southern Hemisphere warming. Each experiment is started from the glacial equilibrium climate and is integrated until a quasi steady state is reached. All experimental time series are smoothed by a one-year boxcar-average.

Freshwater pulse experiments

The experiments in Fig. 4a simulate deglacial meltwater discharge to the Atlantic Ocean between 20°N and 50°N. Experiment LGM_CTRL_H500 and LGM_SH_H500 display the model response to a 500-year freshwater-pulse of 0.15 Sv. The starting point of experiment LGM_SH_Hperm, representing the THC 'off-mode', results from a permanent freshwater flow of 0.15 Sv to the glacial equilibrium state. The freshwater flow persists during this experiment. In LGM_SH_H500 and LGM_SH_Hperm, Southern Hemisphere warming is executed as in LGM_100, while the glacial background conditions in experiment LGM_CTRL_H500 remain unaltered.

Stability analysis

We apply a slowly varying freshwater anomaly with a rate of 5×10^{-5} Sv yr^{-1} (1×10^{-6} Sv yr^{-1} at the transition of the hysteresis curve that starts from LGM_100) uniformly between 20° N and 50° N to the Atlantic Ocean. Integration starts at the upper branches with zero freshwater forcing, which is then increased up to 0.2 Sv and 0.32 Sv for LGM_CTRL and LGM_100, respectively. The integration proceeds on the lower branch with freshwater input decreasing until −0.12 Sv. Then the freshwater increases again to close the loops. Owing to the slowly varying nature of the surface forcing the model is in quasi-equilibrium during the integration.

Received 21 November 2002; accepted 23 June 2003; doi:10.1038/nature01855.

1. Sowers, T. & Bender, M. Climate records covering the last deglaciation. *Science* **269**, 210–214 (1995).
2. Petit, R. *et al.* Climate and atmospheric history of the past 420,000 years from the Vostok ice core, Antarctica. *Nature* **399**, 429–436 (1999).
3. Marshall, J. S. & Clarke, G. K. C. Modelling North American freshwater runoff through the last glacial cycle. *Quat. Res.* **52**, 300–315 (1999).
4. Stocker, T. F. & Wright, D. G. Rapid transitions of the ocean's deep circulation induced by changes in surface water fluxes. *Nature* **351**, 729–732 (1991).
5. Maier-Reimer, E., Mikolajewicz, U. & Hasselmann, K. Mean circulation of the Hamburg LSG OGCM and its sensitivity to the thermohaline surface forcing. *J. Phys. Oceanogr.* **23**, 731–757 (1993).
6. Sarnthein, M. *et al.* Changes in east Atlantic deepwater circulation over the last 30,000 years: Eight time slice reconstructions. *Paleoceanography* **9**, 209–267 (1994).
7. Prange, M., Romanova, V. & Lohmann, G. The glacial thermohaline circulation: Stable or unstable? *Geophys. Res. Lett.* **29**, 10.1029/2002GL015337 (2002).
8. Shemesh, A. *et al.* Sequence of events during the last deglaciation in Southern Ocean sediments and Antarctic ice cores. *Paleoceanography* **17**, 101029/2000PA000599 (2002).
9. Gordon, A. L., Weiss, R. F., Smethie, W. M. Jr & Warner, M. J. Thermocline and intermediate water communication between the South Atlantic and Indian Oceans. *J. Geophys. Res.* **97**, 7223–7240 (1992).
10. Broecker, W. S. The great ocean conveyor. *Oceanography* **4**, 79–89 (1991).
11. Shin, S. I., Otto-Bliesner, B., Brady, E. C., Kutzbach, J. E. & Harrison, S. P. A simulation of the last glacial maximum climate using the NCAR-CCSM. *Clim. Dyn.* **20**, 127–151 (2003).
12. Ganopolski, A. & Rahmstorf, S. Rapid changes of glacial climate simulated in a coupled climate model. *Nature* **409**, 153–158 (2001).
13. Macdonald, A. M. & Wunsch, C. An estimate of global ocean circulation and heat fluxes. *Nature* **382**, 436–439 (1996).
14. Weijer, W., De Ruijter, W. P. M., Sterl, A. & Drijfhout, S. S. Response of the Atlantic overturning circulation to South Atlantic sources of buoyancy. *Glob. Planet. Change* **34**, 293–311 (2002).
15. Stommel, H. Thermohaline convection with two stable regimes of flow. *Tellus* **13**, 224–230 (1961).
16. Stocker, T. F. in *Continuum Mechanics and Applications in Geophysics and the Environment* (eds Straugham, B., Greeve, R., Ehrentraut, H. & Wang, Y.) 337–367 (Springer, New York, 2001).
17. Rühlemann, C., Mulitza, S., Müller, P. J., Wefer, G. & Zahn, R. Warming of the tropical Atlantic Ocean and slowdown of thermohaline circulation during the last deglaciation. *Nature* **402**, 511–514 (1999).
18. Bard, E., Rostek, F., Turon, J. L. & Gendreau, S. Hydrological impact of Heinrich events in the subtropical northeast Atlantic. *Science* **289**, 1321–1324 (2000).
19. Sachs, J. P., Anderson, R. F. & Lehman, S. J. Glacial surface temperatures of the southeast Atlantic Ocean. *Science* **293**, 2077–2079 (2001).
20. Crowley, T. J. North Atlantic Deep Water cools the Southern Hemisphere. *Paleoceanography* **7**, 489–497 (1992).
21. Stephens, B. B. & Keeling, R. F. The influence of Antarctic sea ice on glacial–interglacial CO_2 variations. *Nature* **404**, 171–174 (2000).
22. Toggweiler, J. R. Variation of atmospheric CO_2 by ventilation of the ocean's deepest water. *Paleoceanography* **14**, 571–588 (1999).
23. Lohmann, G. & Schulz, M. Reconciling Bølling warmth with peak deglacial meltwater discharge. *Paleoceanography* **15**, 537–540 (2000).
24. Schott, W. Die Foraminiferen in dem äquatorialen Teil des Atlantischen Ozeans. *Deut. Atl. Exped. Meteor* 1925–1927 **3**, 43–134 (1935).
25. Berger, W. H. & Wefer, G. in *The South Atlantic: Present and Past Circulation* (eds Wefer, G., Berger, W. H., Siedler, G. & Webb, D. J.) 363–410 (Springer, Heidelberg, 1996).
26. Kim, S. J., Crowley, T. J. & Stössel, A. Local orbital forcing of Antarctic climate change during the last interglacial. *Science* **280**, 728–730 (1998).
27. Koutavas, A., Lynch-Stieglitz, J., Marchitto, T. M. Jr & Sachs, J. P. El Niño-like pattern in ice age tropical Pacific sea surface temperature. *Science* **297**, 226–230 (2002).
28. Schouten, M. W., De Ruijter, P. M. & van Leeuwen, P. J. Upstream control of Agulhas Ring shedding. *J. Geophys. Res.* **107** 101029/2001JC000804 (2002).
29. Prange, M., Lohmann, G. & Paul, A. Influence of vertical mixing on the thermohaline hysteresis: Analyses of an OGCM. *J. Phys. Oceanogr.* **33**, 1707–1721 (2003).
30. Lohmann, G. & Lorenz, S. The hydrological cycle under paleoclimatic boundary conditions as derived from AGCM simulations. *J. Geophys. Res.* **105**, 17417–17436 (2000).

Supplementary Information accompanies the paper on **www.nature.com/nature**.

Acknowledgements We thank H. Jansen, S. Mulitza and M. Prange for suggestions. L. Könnecke, S. Schubert, M. Butzin and S. Blessing are acknowledged for their technical support. This work was supported by BMBF through the DEKLIM project 'climate transitions'.

Competing interests statement The authors declare that they have no competing financial interests.

Correspondence and requests for materials should be addressed to G.K. (gregor.knorr@dkrz.de).

Possible thermal and chemical stabilization of body-centred-cubic iron in the Earth's core

Lidunka Vočadlo[1], Dario Alfè[1,2], M. J. Gillan[2], I. G. Wood[1], J. P. Brodholt[1] & G. David Price[1]

[1]*Research School of Earth Sciences, Birkbeck College and University College London, and*
[2]*Department of Physics and Astronomy, University College London, Gower Street, London WC1E 6BT, UK*

The nature of the stable phase of iron in the Earth's solid inner core is still highly controversial. Laboratory experiments[1] suggest the possibility of an uncharacterized phase transformation in iron at core conditions and seismological observations[2–4] have indicated the possible presence of complex, inner-core layering. Theoretical studies[5,6] currently suggest that the hexagonal close packed (h.c.p.) phase of iron is stable at core pressures and that the body centred cubic (b.c.c.) phase of iron becomes elastically unstable at high pressure. In other h.c.p. metals, however, a high-pressure b.c.c. form has been found to become stabilized at high temperature. We report here a quantum mechanical study of b.c.c.-iron able to model its behaviour at core temperatures as well as pressures, using *ab initio* molecular dynamics free-energy calculations. We find that b.c.c.-iron indeed becomes entropically stabilized at core temperatures, but in its pure state h.c.p.-iron still remains thermodynamically more favourable. The inner core, however, is not pure iron, and our calculations indicate that the b.c.c. phase will be stabilized with respect to the h.c.p. phase by sulphur or silicon impurities in the core. Consequently, a b.c.c.-structured alloy may be a strong candidate for explaining the observed seismic complexity of the inner core[2–4].

Seismic measurements show that the Earth's solid inner core is complex. The detailed interpretations of these data differ, but all workers[2–4] conclude that the inner core exhibits a significant degree of layering, which may either reflect the changing history of core crystallization, or the occurrence of an unidentified change in the core-forming phase. It is currently generally accepted that the core consists predominantly of Fe, and conventional interpretations of the elastic anisotropy of the inner core have been based on the idea of a partial alignment of crystals of h.c.p.-Fe[5]. Recently, however this interpretation has been challenged[3], as has the assumption that h.c.p.-Fe is the thermodynamically stable polymorph of Fe at the high temperatures found in the inner core[1]. The low pressure (P)–temperature (T) phase diagram of Fe is not controversial, with b.c.c.-Fe stable at ambient conditions, h.c.p.-Fe stable above about 15 GPa at low temperatures and the face-centred-cubic (f.c.c.) structure being stable above about 1,300 K at low pressures. High-P/T diamond-anvil-cell experiments[7] suggest a new phase above ~40 GPa and ~1,000 K, but the structure of this phase is still unresolved. In addition, a solid–solid phase transition at around